# CrossMark

#### ORIGINAL ARTICLE

# Shoaling internal waves may reduce gravity current transport

Charlie A. R. Hogg<sup>1</sup> • Galen C. Egan<sup>1</sup> · Nicholas T. Ouellette<sup>1</sup> · Jeffrey R. Koseff<sup>1</sup>

Received: 8 March 2017/Accepted: 23 October 2017/Published online: 3 November 2017 © Springer Science+Business Media B.V. 2017

Abstract Gravity currents descending along slopes have typically been studied in quiescent environments, despite the fact that in many geophysical settings there is significant externally driven motion. Here we investigate how the head of a gravity current is influenced by interfacial internal waves at the pycnocline of a two-layer ambient water column. Our experimental measurements show that larger amplitude internal waves, interacting with the gravity current, reduce both the mass transport by the gravity current and its thickness. These results suggest that the ambient internal wave field should be considered when estimating transport by gravity currents in geophysical settings with strong internal waves, such as lakes and the coastal ocean.

**Keywords** Gravity currents · Internal waves · Desalination · Coastal ocean processes · Limnology · River inflows

## 1 Introduction

Gravity currents interact with internal waves in a host of natural settings, such as dense river inflows into lakes [9, 16, 21, 39], benthic turbidity currents [27, 29, 31] or katabatic winds [40]. Anthropogenic gravity currents in the coastal environment, such as the discharge of brine effluents from seawater desalination facilities [20, 25], are also becoming more commonplace. The extent to which dense brine discharges (referred to here as brine gravity currents) from these facilities impact the coastal ocean remains very uncertain [15, 25], but may have significant ecological and economic consequences [26]. Therefore, fundamental understanding of the mixing and transport of the gravity currents in the ambient receiving waters, which typically have strong internal wave action, is critical to

Bob and Norma Street Environmental Fluid Mechanics Laboratory, Stanford University, Stanford, CA, USA



<sup>☐</sup> Charlie A. R. Hogg chogg@cantab.net

predicting the concentrations of brine and chemical additives in the currents and the reduction in oxygen at the sea bed beneath the brine [20].

Typically, gravity currents are nearly horizontal flows driven by density gradients [41]. When the gravity current is on a slope or incline, it entrains ambient water and is gradually diluted as it flows [8, 11, 13, 14, 17]. When the ambient water is stratified, fluid from the gravity current will intrude into the ambient at heights of neutral buoyancy [4, 23, 43], whereas in two-layer stratifications, a gravity current will intrude at the pycnocline if it is lighter than the lower layer, or will split into an intrusion at the pycnocline and a gravity current descending beneath the lower ambient layer (see Fig. 1) if it contains fluid denser than the lower layer [9, 33, 40, 48].

If we introduce internal waves into the receiving environment the picture becomes more complex. For example, qualitative observations have suggested that the volume exchange between the gravity current and the ambient water by entrainment and detrainment can be influenced by internal waves in the ambient [3, 9, 21, 22, 49]. However, even though internal waves are known to be a significant source of kinetic energy in the benthic environment [16, 24, 29, 30, 37, 42] there are currently few quantitative measurements of the influence of internal waves on these exchanges. Evidence for the influence of internal waves on gravity current transport was found in the field by Fischer and Smith [16], plotted in their Fig. 4. This showed that, when internal waves led to upwelling of the hypolimnion, some of the initially dense river water was transported into the surface layer whilst the rest of the river water continued as an underflow. The river-borne nutrients then became available for primary production resulting in problematic algal growth. Whilst they conclude that internal wave motions may play a strong role in the transport of nutrients to the surface waters, this has not subsequently been incorporated into inflow models.

In isolation, internal waves incident on shelf slopes have been studied intensively in laboratory experiments [5, 18, 19, 35, 36], numerical simulations [1, 2, 6, 7, 44, 45] and field observations [7, 12, 37, 46], revealing that a number of different outcomes are possible when a wave encounters a slope. When the wave is shallow compared to the bathymetric slope, it will form a seiche rather than break, reflecting most of the incident wave energy [6, 32, 46]. For steeper interfacial internal waves, such as those investigated here, the incident wave will break to form either a coherent bolus or a turbulent surge propagating upslope. Prior work has also shown that, depending on the wave steepness, the wave can break through distinct backward breaking, top-breaking or forward breaking mechanisms [5, 35].

Our goal in this paper is to begin to identify and quantitatively describe the influence of internal waves on gravity currents, focusing specifically on the modification to the

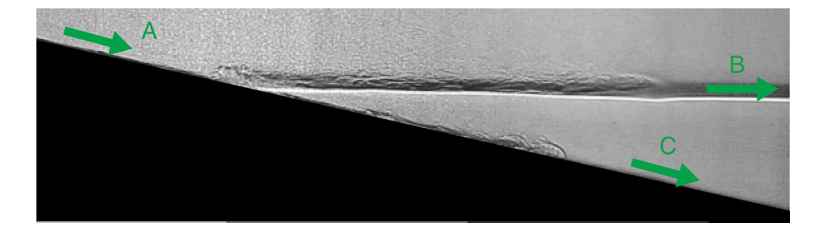


Fig. 1 A shadowgraph image of an inclined gravity current descending (a) through a two-layer ambient. The gravity current splits at the pycnocline, with the lighter part intruding at the pycnocline (b) and the densest part descending as an underflow beneath the lower layer (c). These motions are highlighted by the arrows



downslope mass flux. The particular experiments described here investigate how an internal wave at a density interface modifies the flow of an inclined gravity current passing through the interface in a two-layer ambient environment. To allow the gravity current to descend through the pycnocline, the bottom of the basin must be inclined. Because it is important to identify how strong the ambient motion needs to be relative to the strength of the gravity current in altering the transport by the gravity current, we performed the experiments over a range of wave amplitudes. The apparatus was designed to produce an internal wave that was repeatable, easily characterized and similar to those observed in the coastal ocean [46].

We continue below in Sect. 2 by describing the experimental apparatus and the methods used in the experiments. In Sect. 3 we present our results, showing the variation in the gravity current characteristics for increasing wave amplitudes, and discussing the mechanism by which the internal wave modifies the gravity current. Finally, we summarize our conclusions and describe how we plan to further investigate the influence of ambient motion on underflows.

### 2 Facilities and methods

A tank apparatus, shown in Fig. 2, was set up to generate an internal wave that would shoal on the slope while the inclined gravity current was passing through the pycnocline. The tank is 0.15 m in breadth, 1.2 m in length, and 0.2 m in height, and was inclined at an angle  $\theta = 5.4^{\circ}$  from the horizontal. The fluid in the tank was stratified with two distinct layers. The upper layer was fresh water, with density  $\rho_1$ ; the lower layer had a higher density  $\rho_2$ , achieved by adding sodium chloride for a salinity of 20.2 parts per thousand (ppt). The thickness of the interface (pycnocline) was approximately 1 cm. Salinities were measured with an Anton-Paar density meter, and the variation was less than 0.1 ppt. The experiments were performed in the following way. First, upper layer fluid was extracted from behind the internal wave lock with a syringe to allow the pycnocline behind the lock to rise: this set the conditions for the internal wave to be released by the lock. The raised height, a, of the pycnocline behind the lock was varied in different runs and was the control parameter used to vary the strength of the wave. The fluid in the gravity current lock (density  $\rho_3$ ) had a salinity of 25.1 ppt. The relative timing of the release of the two locks was kept approximately constant throughout the runs; the small uncertainty in timing due to the manual release of the locks was negligible on the time scale of the flow development. This

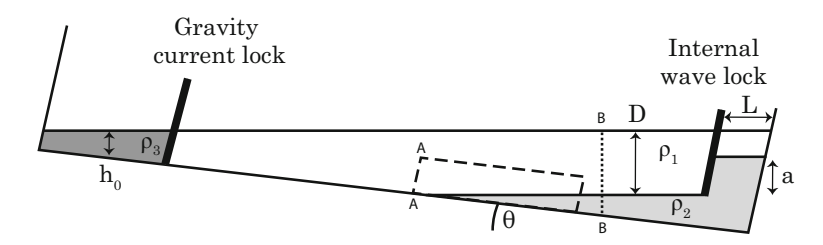


Fig. 2 Schematic of experimental apparatus. Locks were pulled out to release the internal wave and the gravity current. The vertical interrogation plane is shown by the dotted line (with length  $h_f = 84$  mm) and the image window is shown by the dashed rectangle. The internal wave lock height a was varied for each experimental run; the other geometric parameters were fixed at  $\theta = 5.4^{\circ}$ ,  $h_0 = 25$  mm, L = 124 mm, and D = 54 mm



timing was fixed to ensure that the internal wave reached the head of the gravity current shortly after the gravity current head had passed through the pycnocline and travelled as an underflow beneath the lower layer of ambient fluid. While we recognize that the relative timing of the releases is a key experimental parameter that can affect the outcome of the experiments, we chose to reduce the complexity of this initial set of experiments by keeping the timing constant. It will be investigated in future work.

The concentration of the gravity current fluid was measured during the experiments using planar laser induced fluorescence (PLIF). A fluorescent dye (Rhodamine 6G) was added to the initial gravity current fluid at a known concentration. A light sheet (approximately 3 mm thick) was produced along the center of the tank by passing a 532 nm laser beam produced by a CivilLaser LSR532H-2W laser through a cylindrical lens and illuminating the water column through the base of the tank. The illuminated part of the tank was imaged using a Imperx Bobcat ICL-B2520 CCD camera acquiring images at 16 frames per second with an exposure time of 20 ms. The size of the images acquired during the experiments was 180 mm by 150 mm and the camera had an array of 2456 by 2058 pixels, giving a resolution of 13 pixels per mm. The light intensity imaged by the camera was converted to a dye concentration with a calibration using a uniform dye field as described by Crimaldi and Koseff [10]. As dye was only introduced into the source of the gravity current, the dye concentration can be used to estimate the mass flux of the gravity current source fluid. The index of refraction of the different fluids was not matched in these experiments because particle tracking techniques were not used for these experiments. The signal from the bulk flux of dyed fluid was not affected by index of refraction issues.

The incident internal wave can be characterized by a wave Froude number  $Fr_w = a/L$ , where L is the length of the lock release. This parameter describes the ratio of the fluid velocity to the wave speed: the larger the Froude number, the steeper the wave. In these experiments,  $Fr_w$  was varied between 0 and 0.29. The lock length at the initial release was L=124 mm and the amplitude in each case is shown in Table 1. The other geometric parameters were held fixed for each experiment, with  $\theta=5.4^\circ$ ,  $h_0=25$  mm, L=124 mm, and D=54 mm (see Fig. 2). In the coastal ocean, shoaling internal waves can realistically have  $Fr_w$  of the order of 0.1 [46]. The gravity current release can be characterized by the density Richardson number  $Ri_\rho=g_i'D/(g_c'h_0)$ , where  $g_i'=g(\rho_2-\rho_1)/\rho_r$  is the reduced gravity at the interface, D is the depth of the upper layer,  $g_c'=\frac{1}{2}$ 

Table 1	Parameter	values for
experime	ntal runs	

Run ID	Initial lock height $a$ (m)	$Fr_w$
1	0	0
2	0	0
3	0.012	0.10
4	0.012	0.10
5	0.018	0.15
6	0.024	0.19
7	0.024	0.19
8	0.024	0.19
9	0.03	0.24
10	0.036	0.29
11	0.036	0.29
12	0.036	0.29

Only the initial lock height a (see Fig. 2) was varied from run to run, with all other parameters held constant. The density Richardson number  $Ri_{\rho}$  was 3.9 for all runs



 $g(\rho_3 - \rho_1)/\rho_r$  is the reduced gravity of the gravity current source fluid in the upper layer,  $2h_0$  is the initial depth of the gravity current source fluid in the lock, g is acceleration due to gravity and  $\rho_r = 1000$  kg m<sup>-3</sup> is a reference density. In these experiments,  $Ri_\rho$  for the gravity current fluid was held fixed at 3.9. For a discharge from a desalination plant to the coastal ocean, realistic values would be of the order of  $g'_i = 0.004$  ms<sup>-2</sup>,  $g'_c = 0.01$  ms<sup>-1</sup>, D = 20 m and  $h_0 = 2$  m, giving  $Ri_\rho = 4$  [28, 47].

#### 3 Results

# 3.1 Gravity current mass flux and thickness

To characterize the gravity current mass transport in different wave conditions, integral measures of the mass flux per unit width of source gravity current fluid and the gravity current thickness were used. These estimates were evaluated on a vertical interrogation plane 0.55 m downslope from the gravity current lock, indicated by the dotted line B–B in Fig. 2. At this location, the gravity current had flowed far enough beneath the pycnocline for the gravity current fluid to be separated by lower layer fluid from any intrusion at the pycnocline. The mass flux in the gravity current was calculated by averaging the mass flux over a period of T=5 s beginning just after the gravity current head reached the interrogation plane. The period of 5 s was chosen because it was long enough for the wave to pass over the gravity current, but not long enough for the mixing to be influenced by the reflection of waves from the end wall of the tank, or for the intrusion at the pycnocline to reach the interrogation plane. We examined the sensitivity of the averaging period on our results and found that over a reasonable range the period did not affect our results.

The mass flux of source gravity current fluid,  $\dot{m}$ , was estimated as

$$\dot{m} = U_f \cos \theta \int_0^{h_f} c dh', \tag{1}$$

where  $U_f$  is the average speed of the front of the gravity current,  $h_f$  is the height of the free surface, c is the local dye concentration, and h' is the vertical distance above the tank bottom to the location of the measurement. In the plots of  $\dot{m}$  that follow, the local dye concentration c was normalized against  $c_0$ , the concentration in the head when it first reaches the interrogation plane. The speed of the front of gravity current  $U_f$  was averaged over the time it took for the front to pass through the field of view of the camera. This estimate of the mass flux is based on the assumption that the velocity is uniform across the height of the gravity current and constant in time. The thickness of the current was estimated as

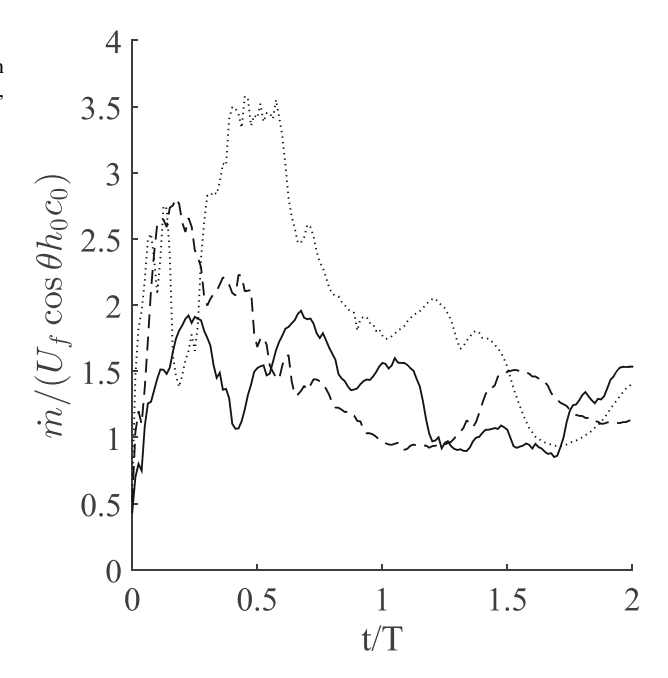
$$H = \frac{\int_0^{h_f} ch'dh'}{\int_0^{h_f} cdh'},\tag{2}$$

where  $h_f = 84$  mm at the interrogation plane (see Fig. 2). In the case of a gravity current with a top-hat density profile, in which the density is uniform over the thickness of the gravity current, H gives half the thickness of the top-hat profile.

The time series of the mass flux, non-dimensionalized by the flux  $U_f h_0 c_0$ , is plotted in Fig. 3 for three different cases. Here,  $c_0$  is the concentration in the head when it first reaches the interrogation plane. The plot shows that with no wave present the mass flux



Fig. 3 Time series of mass flux passing the interrogation plane in run 1 with no wave (dotted line), run 5 with wave of  $Fr_w = 0.14$  (dashed line) and run 10 with wave of  $Fr_w = 0.29$  (solid line)



peaked as the head at the front of the current initially passed the interrogation plane and then reduced to a lower level in the tail of the current after t/T=1. When a wave was incident on the current, the initial peak in mass flux associated with the head of the gravity current was reduced. The mass flux in the tail of the gravity current was not significantly altered. As the  $Fr_w$  of the incident wave was increased, the magnitude of the initial peak in mass flux reduced until, for the largest wave generated in our apparatus, the mass flux in the initial part of the gravity current was approximately that of the tail. This (and the images shown later in Fig. 6) suggests that the wave stripped the dilute fluid in the gravity current head from the current and transported it upslope, leaving only the lower part of the current present in the tail.

The time series show substantial fluctuations, caused by the passing of turbulent eddies in the gravity current, and so, as one would expect, runs with the same initial conditions did not produce identical time series of mass flux. However, the trend of the reduced peak in mass flux with  $Fr_w$  was shown consistently in repeated trials, as shown by the three example time series at  $Fr_w = 0.29$  plotted in Fig. 4. Figure 5a shows that the variation in the time averaged mass flux between these three repeat runs is much smaller than the variation over the range of  $Fr_w$ .

The average mass flux  $\bar{m}$  and average current thickness  $\bar{H}$  over the duration T for different incident wave amplitudes are plotted in Fig. 5a, b. It is clear from the data that both the mass flux and current thickness decrease as the amplitude of the incident wave increased. The presence of the largest wave suppressed the average mass flux by 40%, and the average current thickness by 30%, compared with the case with no wave. This observation is consistent with our interpretation that the wave stripped the dilute fluid in the gravity current head and transported this fluid upslope, thus reducing the mass transport and the thickness at the head of the current. The data also suggest that the reduction in mass



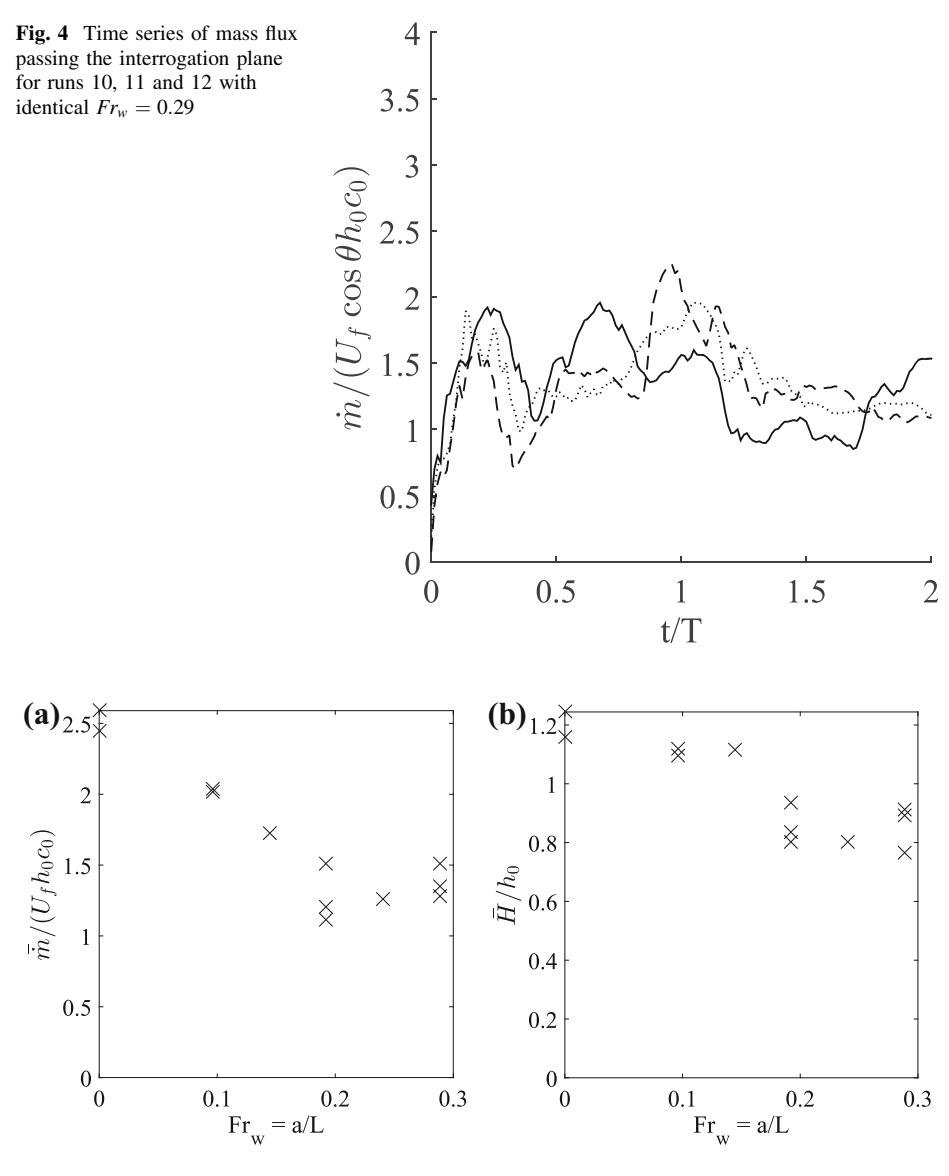


Fig. 5 Trends in a average mass flux and b average current thickness with wave Froude number

flux and thickness may saturate above  $Fr_w = 0.2$ . To test this conjecture, larger-amplitude waves are needed, which in turn require a larger tank than we have used here.

# 3.2 Spatial distribution during wave-current interaction

To more fully understand the mechanisms by which the wave reduces the thickness of the gravity current, we made qualitative observations over a larger field of view where we could image the full interaction of the wave with the gravity current, shown by the dashed rectangle in Fig. 2. In these visualizations, dye was added to the lower ambient layer and



the gravity current in proportion to their respective salt concentrations, so that the motion of the wave at the pycnocline could be visualized simultaneously with the motion of the gravity current. Snapshots of the dye concentration are shown in Fig. 6 panels a–d and e–h for experimental cases with no wave and with  $Fr_w = 0.29$ , respectively. In both cases, the first snapshot is 2.1 s after the currents enter the left of the image plane (line A–A on Fig. 2) and are shown subsequently at 1.7 s intervals. A light blue contour indicates a dye concentration midway between the initial lower layer concentration and the gravity current source concentration. For an experiment with no incident wave, Fig. 6a shows the gravity current shortly after the gravity current head passed through the pycnocline. The pycnocline then rose as the gravity current flowed beneath the lower ambient layer, as was seen in similar experiments conducted by Monaghan et al. [34]. The gravity current then continued down the slope whilst a wave of elevation at the pycnocline moved with the current, shown in Fig. 6b–d. At all times, the thicker head structure at the front of the gravity current is noticeably present as the gravity current moved down the slope beneath the lower layer.

The evolution of the gravity current in the presence of a wave is shown in Fig. 6e-h and is described in the following text. In Fig. 6e the gravity current had just reached the pycnocline. At the right hand side of the frame in Fig. 6f, the pycnocline was slightly inclined towards the left by the oncoming internal wave. In addition, as the gravity current

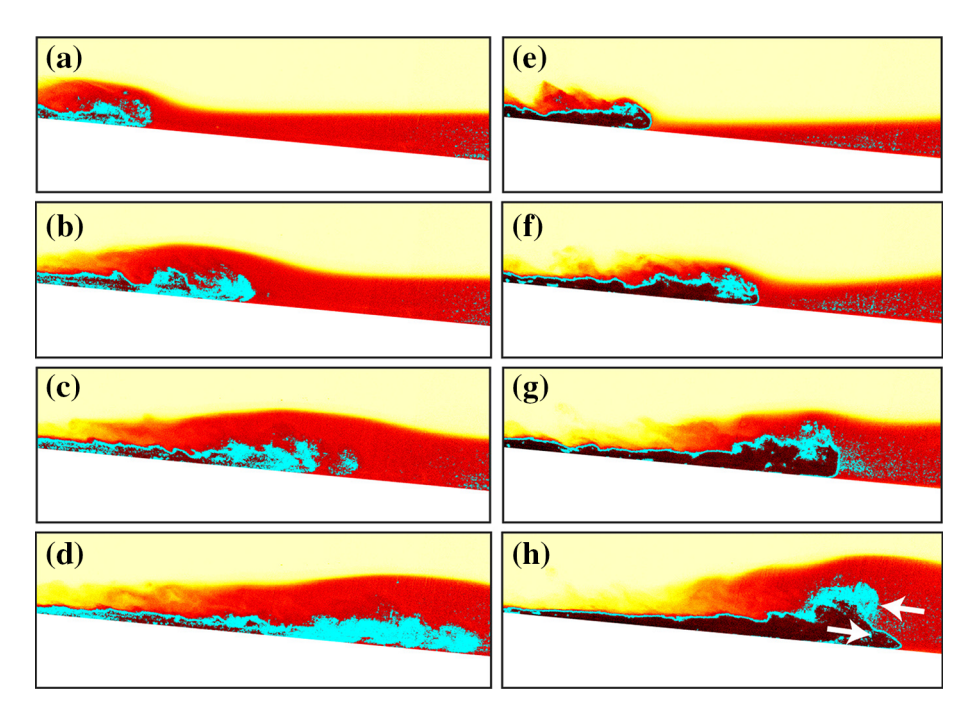


Fig. 6 Snapshots of density field at 1.7 s intervals during gravity current passing through the pycnocline. The image window is 30.0 cm in width. The colormap shows dense fluid with  $c/c_0=1$  as dark red and light fluid with  $c/c_0=0$  as pale yellow. Panels  ${\bf a}$ - ${\bf d}$  show a run with no internal wave and panels  ${\bf e}$ - ${\bf h}$  show a run with a shoaling wave of  $Fr_w=0.29$ . The cyan contour shows the concentration of fluid half way between the lower layer and the gravity current source fluid. The upper white arrow in  ${\bf h}$  shows the upslope motion induced by the internal wave pushing the upper part of the head fluid back. The lower white arrow shows the motion in the lower part of the gravity current, which continues to move down the slope



passed through the pycnocline and flowed into the lower layer, the pycnocline was displaced upwards, just as occurred in the case with no wave. The thick head of the gravity current was also visible at this point. In Fig. 6g the head of the gravity current is made thicker as the wave moves over the gravity current. This was caused by the velocity field associated with the wave moving to the left immediately beneath the pycnocline. A similar thickening of the head was also observed by Robinson et al. [38] in surface waves above a gravity current traveling in the opposite direction from the incident waves, suggesting that this thickening may be a general response to a gravity current traveling beneath an interfacial wave moving in the opposite direction. Figure 6h shows that the fluid in the upper part of the head was held back by the upslope motion caused by the passing wave. This could be described as the head of the gravity current being "decapitated" by the passing wave. The lower part of the current, which has approximately the same thickness as the tail of the gravity current, continues to move down the slope. This effect also results in the thinning of the front portion of the gravity current (Fig. 6h) which appears to be squeezed by the presence of the internal wave as it continues to travel down the slope. This process of moving dilute fluid in the head upslope and leaving a thinner gravity current head appears to be the mechanism by which the internal wave reduces the mass flux in the gravity current, as seen in the trends in Fig. 5a. The shoaling internal wave went on to form a bolus, which moved up the slope before falling back down. At times after that shown in Fig. 6h, reflections from the back wall of the tank contaminated the influence of the internal solitary wave on the gravity current. Furthermore, previous work [22] has suggested that when the internal wave moves the gravity current fluid up into the upper ambient layer, the gravity current fluid mixes with fluid from the upper ambient layer. This mixing increases the amount of gravity current fluid that is neutrally buoyant at the pycnocline, thus permanently reducing the flux of current into the lower layer. The added displacement of the pycnocline above the head of the gravity current compared to the case without a wave (compare, for example, Fig. 6d with h) is caused by the superposition of the incident internal wave with the wave created by the gravity current.

#### 4 Discussion and conclusions

Our experiments show that incident internal waves can have a significant influence on the mass transported by a gravity current. As the amplitude of the internal wave was increased we observed a progressive reduction in the average mass flux of the source gravity current fluid and the thickness of the gravity current. Specifically, the mass flux in the initial part of the gravity current was reduced by 40% when the largest wave produced in this study,  $Fr_w = 0.29$ , was incident on the slope. Images of the full concentration field suggest that the mechanism for the internal wave altering the gravity current is that the velocity field induced by the internal wave passing over the head of the gravity current strips part of the gravity current head and then moves this upper recirculating part of the gravity current head upslope. Only the lower part of the gravity current continued to travel downslope.

In the observations of Fischer and Smith [16], internal wave motion was observed to redirect gravity current fluid to the surface of the lake. Whilst Fischer and Smith considered a different configuration, where gravity current fluid was raised to the surface of the lake, it is likely that the upslope motion of the shoaling internal gravity wave, as we observed here in the lab, caused the change in the gravity current transport. Measurements in the field with finer time resolution, such as those by Bourgault et al. [7] would allow the



mechanisms observed in the lab to be better compared to processes in the field. Calculations on the impact of internal waves on dense inflows by Cortés et al. [9] considered a regime where the velocities generated at the bed by the internal wave field  $U_i$  were an order of magnitude smaller than the velocity of the gravity current front  $U_u$ . In the regime investigated in our experiments the velocities generated by the internal wave field were of a similar order of magnitude to gravity current front velocity. This meant that the shear generated by the internal waves was substantial enough to separate the upper part of the fluid in the head from the front of the gravity current. Field settings with larger density drops at the pycnocline and shallower bed slopes than in the Cortés et al. [9] study will operate in a regime more similar to our laboratory observations.

In the future, we plan to extend this study by looking at larger amplitude waves in a larger facility and a broader range of conditions of slope angles and time delays between the gravity current and internal wave. The different wave breaking regimes at different slope angles [1] and different phases of the wave breaking motion are likely to have different influences on the gravity current.

**Acknowledgements** We gratefully acknowledge assistance in the lab from Valerie Pietraz, Bill Sabala and Michelle Dutt. This work was supported by National Science Foundation Grant No. OCE—1634389 and the Stanford Woods Institute for the Environment.

#### References

- Aghsaee P, Boegman L, Lamb KG (2010) Breaking of shoaling internal solitary waves. J Fluid Mech 659:289–317. https://doi.org/10.1017/S002211201000248X
- Arthur RS, Fringer OB (2014) The dynamics of breaking internal solitary waves on slopes. J Fluid Mech 761:360–398. https://doi.org/10.1017/jfm.2014.641
- Baines PG (2001) Mixing in flows down gentle slopes into stratified environments. J Fluid Mech 443:237–270
- Baines PG (2008) Mixing in downslope flows in the ocean—plumes versus gravity currents. Atmos Ocean 46(4):405–419. https://doi.org/10.3137/AO925.2008
- Boegman L, Ivey GN, Imberger J (2005) The degeneration of internal waves in lakes with sloping topography. Limnol Oceanogr 50(5):1620–1637. https://doi.org/10.4319/lo.2005.50.5.1620
- Bourgault D, Kelley DE (2007) On the reflectance of uniform slopes for normally incident interfacial solitary waves. J Phys Oceanogr 37(5):1156–1162. https://doi.org/10.1175/JPO3059.1
- Bourgault D, Blokhina MD, Mirshak R, Kelley DE (2007) Evolution of a shoaling internal solitary wavetrain. Geophys Res Lett 34(3):L03,601. https://doi.org/10.1029/2006GL028462
- Cenedese C, Adduce C (2010) A new parameterization for entrainment in overflows. J Phys Oceanogr 40(8):1835–1850. https://doi.org/10.1175/2010JPO4374.1
- Cortés A, Fleenor WE, Wells MG, de Vicente I, Rueda FJ (2014) Pathways of river water to the surface layers of stratified reservoirs. Limnol Oceanogr 59(1):233–250
- Crimaldi J, Koseff J (2001) High-resolution measurements of the spatial and temporal scalar structure of a turbulent plume. Exp Fluids 31(1):90–102
- Dallimore CJ, Imberger J, Ishikawa T (2001) Entrainment and turbulence in saline underflow in Lake Ogawara. J Hydraul Eng 127:937–948
- Davis KA, Monismith SG (2011) The modification of bottom boundary layer turbulence and mixing by internal waves shoaling on a barrier reef. J Phys Oceanogr 41(11):2223–2241. https://doi.org/10.1175/ 2011JPO4344.1
- 13. Ellison TH, Turner JS (1959) Turbulent entrainment in stratified flows. J Fluid Mech 6(03):423-448
- Fernandez RL, Imberger J (2006) Bed roughness induced entrainment in a high Richardson number underflow. J Hydraul Res 44(6):725–738. https://doi.org/10.1080/00221686.2006.9521724
- Fernández-Torquemada Y, Gónzalez-Correa JM, Loya A, Ferrero LM, Díaz-Valdés M, Sánchez-Lizaso JL (2009) Dispersion of brine discharge from seawater reverse osmosis desalination plants. Desalin Water Treat 5(1–3):137–145



- Fischer HB, Smith RD (1983) Observations of transport to surface waters from a plunging inflow to Lake Mead. Limnol Oceanogr 28(2):258–272. https://doi.org/10.4319/lo.1983.28.2.0258
- Hebbert B, Imberger J, Loh I (1979) Collie river underflow into the Wellington reservoir. J Hydraul Div ASCE 105:533–545
- Helfrich KR (1992) Internal solitary wave breaking and run-up on a uniform slope. J Fluid Mech 243:133–154. https://doi.org/10.1017/S0022112092002660
- Helfrich KR, Melville WK (1986) On long nonlinear internal waves over slope-shelf topography.
  J Fluid Mech 167:285–308. https://doi.org/10.1017/S0022112086002823
- Hodges BR, Furnans JE, Kulis PS (2011) Thin-layer gravity current with implications for desalination brine disposal. J Hydraul Eng 137(3):356–371. https://doi.org/10.1061/(ASCE)HY.1943-7900.0000310
- Hogg C (2014) The flow of rivers into lakes: experiments and models. Ph.D. thesis, Cambridge University https://doi.org/10.17863/CAM.32
- Hogg CAR, Egan GC, Ouellette NT, Koseff JR (2016) The influence of a shoaling internal gravity wave on a dense gravity current. In: 8th International symposium on stratified flows, San Diego, CA, USA
- Hogg CAR, Dalziel SB, Huppert HE, Imberger J (2017) Inclined gravity currents filling basins: the impact of peeling detrainment on transport and vertical structure. J Fluid Mech 820:400–423. https:// doi.org/10.1017/jfm.2017.196
- Imberger J, Hamblin PF (1982) Dynamics of lakes, reservoirs, and cooling ponds. Annu Rev Fluid Mech 14(1):153–187. https://doi.org/10.1146/annurev.fl.14.010182.001101
- Jenkins S, Paduan J, Roberts P, Schlenk D, Weis J (2012) Management of brine discharges to coastal waters recommendations of a science advisory panel. Southern California coastal water research project, Costa Mesa, CA
- Kvitek RG, Conlan KE, Iampietro PJ (1998) Black pools of death: hypoxic, brine-filled ice gouge depressions become lethal traps for benthic organisms in a shallow Arctic embayment. Mar Ecol Prog Ser 162:1–10. https://doi.org/10.3354/meps162001
- MacIntyre S, Flynn KM, Jellison R, Romero JR (1999) Boundary mixing and nutrient fluxes in Mono Lake, California. Limnol Oceanogr 44(3):512–529. https://doi.org/10.4319/lo.1999.44.3.0512
- Marti C, Antenucci J, Luketina D, Okely P, Imberger J (2011) Near-field dilution characteristics of a negatively buoyant hypersaline jet generated by a desalination plant. J Hydraul Eng 137(1):57–65. https://doi.org/10.1061/(ASCE)HY.1943-7900.0000275
- Marti CL, Imberger J (2007) Exchange between littoral and pelagic waters in a stratified lake due to wind-induced motions: Lake Kinneret, Israel. Hydrobiologia 603(1):25–51. https://doi.org/10.1007/ s10750-007-9243-6
- Masunaga E, Fringer OB, Yamazaki H (2015) An observational and numerical study of river plume dynamics in Otsuchi Bay, Japan. J Oceanogr 72(1):3–21. https://doi.org/10.1007/s10872-015-0324-2
- Meiburg E, Kneller B (2010) Turbidity currents and their deposits. Annu Rev Fluid Mech 42:135–156. https://doi.org/10.1146/annurev-fluid-121108-145618
- 32. Michallet H, Ivey GN (1999) Experiments on mixing due to internal solitary waves breaking on uniform slopes. J Geophys Res Oceans 104(C6):13,467–13,477. https://doi.org/10.1029/1999JC900037
- Monaghan JJ (2007) Gravity current interaction with interfaces. Annu Rev Fluid Mech 39(1):245–261. https://doi.org/10.1146/annurev.fluid.39.050905.110218
- 34. Monaghan JJ, RaF Cas, Kos AM, Hallworth M (1999) Gravity currents descending a ramp in a stratified tank. J Fluid Mech 379:39–69. https://doi.org/10.1017/S0022112098003280
- Moore C, Koseff JR, Hult EL (2016) Characteristics of bolus formation and propogation from breaking internal waves on shelf slopes. J Fluid Mech 791:260–283
- Peacock T, Mercier MJ, Didelle H, Viboud S, Dauxois T (2009) A laboratory study of low-mode internal tide scattering by finite-amplitude topography. Phys Fluids 21(12):121,702. https://doi.org/10. 1063/1.3267096
- Pineda J (1994) Internal tidal bores in the nearshore: warm-water fronts, seaward gravity currents and the onshore transport of neustonic larvae. J Mar Res 52(3):427–458. https://doi.org/10.1357/ 0022240943077046
- Robinson TO, Eames I, Simons R (2013) Dense gravity currents moving beneath progressive freesurface water waves. J Fluid Mech 725:588–610. https://doi.org/10.1017/jfm.2013.112
- Rueda FJ, Fleenor WE, de Vicente I (2007) Pathways of river nutrients towards the euphotic zone in a deep-reservoir of small size: uncertainty analysis. Ecol Model 202(3–4):345–361. https://doi.org/10. 1016/j.ecolmodel.2006.11.006
- Samothrakis P, Cotel AJ (2006) Propagation of a gravity current in a two-layer stratified environment.
  J Geophys Res Oceans. https://doi.org/10.1029/2005JC003125
- Simpson JE (1982) Gravity currents in the laboratory, atmosphere, and ocean. Annu Rev Fluid Mech 14(1):213–234. https://doi.org/10.1146/annurev.fl.14.010182.001241



- Toole JM, Schmitt RW, Polzin KL (1994) Estimates of diapycnal mixing in the abyssal ocean. Science 264(5162):1120–1123. https://doi.org/10.1126/science.264.5162.1120
- 43. Turner JS (1986) Turbulent entrainment: the development of the entrainment assumption, and its application to geophysical flows. J Fluid Mech 173:431–471. https://doi.org/10.1017/S0022112086001222
- Venayagamoorthy S, Fringer O (2012) Examining breaking internal waves on a shelf slope using numerical simulations. Oceanography 25(2):132–139. https://doi.org/10.5670/oceanog.2012.48
- 45. Venayagamoorthy SK, Fringer OB (2007) On the formation and propagation of nonlinear internal boluses across a shelf break. J Fluid Mech 577:137–159. https://doi.org/10.1017/S0022112007004624
- Walter RK, Woodson CB, Arthur RS, Fringer OB, Monismith SG (2012) Nearshore internal bores and turbulent mixing in southern Monterey Bay. J Geophys Res. https://doi.org/10.1029/2012JC008115
- Walter RK, Woodson CB, Leary PR, Monismith SG (2014) Connecting wind-driven upwelling and offshore stratification to nearshore internal bores and oxygen variability. J Geophys Res Oceans 119(6):3517–3534. https://doi.org/10.1002/2014JC009998
- 48. Wells MG, Wettlaufer JS (2007) The long-term circulation driven by density currents in a two-layer stratified basin. J Fluid Mech 572:37–58. https://doi.org/10.1017/S0022112006003478
- Wong ABD, Griffiths RW, Hughes GO (2001) Shear layers driven by turbulent plumes. J Fluid Mech 434(1):209–241

